*Highlights (for review)

Hydrothermal carbonization of *Opuntia ficus-indica* cladodes: Role of process parameters on hydrochar properties

Maurizio Volpe[1], Jillian L. Goldfarb[1,2] and Luca Fiori[1*]

1. University of Trento, Department of Civil, Environmental and Mechanical Engineering, via Mesiano 77, 38123 Trento, Italy
2. Boston University, Department of Mechanical Engineering and Division of Materials Science & Engineering, 110 Cummington Mall, Boston MA 02215 USA

Highlights

- Opuntia ficus-indica cladodes possible hydrothermal carbonization biomass feedstock
- Multivariate linear regression demonstrates impact of process variables on yields
- Solid yield and secondary char depend on temperature, residence time, biomass:water
- Hydrochar HHV maximal and volatile matter minimal at intermediate biomass:water
- Calcium oxalate in biomass remains in char, gasifies it at high temperature

* Corresponding author.
Telephone: +39 0461 282692
E-mail address: luca.fiori@unitn.it

Hydrothermal carbonization of *Opuntia ficus-indica* cladodes: Role of process parameters on hydrochar properties

Maurizio Volpe[1], Jillian L. Goldfarb[1,2] and Luca Fiori[1*]

1. University of Trento, Department of Civil, Environmental and Mechanical Engineering, via Mesiano 77, 38123 Trento, Italy
2. Boston University, Department of Mechanical Engineering and Division of Materials Science & Engineering, 110 Cummington Mall, Boston MA 02215 USA

Abstract

Opuntia ficus-indica cladodes is a potential source of solid biofuel from marginal, dry land. Experiments assessed the effects of temperature (180-250 °C), reaction time (0.5-3 h) and biomass to water ratio (B/W; 0.07-0.30) on chars produced via hydrothermal carbonization. Multivariate linear regression demonstrated that all three process parameters are critically important to hydrochar solid yield, while B/W drives energy yield. Heating value increased together with temperature and reaction time and was maximized at intermediate B/W (0.14-0.20).

Microscopy shows evidence of secondary char formed at higher temperatures and B/W ratios. X-ray diffraction and thermogravimetric data suggest that calcium oxalate in the raw biomass remains in the hydrochar; at higher temperatures, the mineral decomposes into CO_2 and may gasify the char.

Keywords: Hydrothermal carbonization; HTC; solid biofuel; Opuntia ficus-indica; hydrochar.

* Corresponding author.
Telephone: +39 0461 282692
E-mail address: luca.fiori@unitn.it

1. Introduction

Environmental issues surrounding fossil fuels have spurred interest in identifying renewable, carbon-neutral fuel replacements. Lignocellulosic biomass, in particular agricultural and agro-industrial wastes, are potential feedstocks for the production of chemicals and fuels, as their use reduces greenhouse gas emissions without competing with land for food crops (Corneli et al., 2016; Volpe et al. 2014). *Opuntia ficus-indica*, a drought-tolerant plat of the cactacee family, was recently suggested by Yang et al. (2015) as a potential feedstock for biofuel production in semi-arid abandoned marginal lands. *Opuntia ficus-indica* is native to Mexico and was naturalized throughout the Mediterranean basin and in the temperate zones of America, Africa, Asia and Oceania. *Opuntia* species are harvested worldwide for the production of fodder and forage and, over the last decades, for their succulent fruits (prickly pears) and young cladodes for human consumption.

At present, depending on the cultivation procedure (rain-fed or well-irrigated) dry matter productivity of *Opuntia* species ranges between 15 and 50 t ha^{-1} $year^{-1}$ (Yang et al., 2015). In Italy, the average annual production of prickly pears amounts to about 85,000 tons, 90% of which is produced in Sicily, with 4,000 ha of cultivated land (ISTAT, 2016). In Sicily alone, between 60,000 and 200,000 t $year^{-1}$ of dry matter related to *Opuntia* could be available for transformation into biofuels from a relatively limited geographic area. Furthermore, the agro-industrial production of *Opuntia* is expected to increase due to the recent discovery that consumption of prickly pears is potentially linked to reductions in percentage body fat, blood pressure, and total cholesterol (Onakpoya et al., 2015). Thus, the cultivation of *Opuntia* species in semi-

arid marginal lands could lead to the simultaneous production of food for human consumption, food supplements, and residual biomass for biofuels.

Santos et al. (2016) recently investigated the chemical composition and use of *Opuntia ficus-indica* cladodes (OC) as a feedstock for the production of bio-ethanol and bio-methane. However, the use of OC for biofuel production must account for its compositional characteristics, especially the high ash and moisture content. *Opuntia* structural ashes range between 8% (Santos et al., 2016) and 23% (Yang et al., 2015) by mass on a dry basis. The high water content (85-94 wt%), low lignin content (8-12 wt%, dry basis) and high fraction of amorphous cellulose (> 80 wt%, dry basis), suggest that OC can be easily decomposed by thermochemical aqueous phase processes with a reduced exogenous water input (as compared to other terrestrial biomasses) (Yang et al., 2015).

During biomass combustion and gasification, a high alkali metals, alkaline earth metals, and silicon content contributes to slagging and fouling of heat transfer surfaces, thus decreasing the overall thermal efficiency (Reza et al., 2013). However, wet thermochemical treatments are receiving considerable attention for the upgrading of moist biomasses to solid biofuels having reduced inorganic content. For example, hydrothermal carbonization (HTC) was recently demonstrated to upgrade: pulp mill waste (Mäkelä et al., 2015; Wikberg et al., 2016), wine industry waste (Pala et al., 2014; Basso et al., 2016), olive mill industry residual biomasses (Álvarez-Murillo et al., 2015; Volpe et al. 2016; Volpe and Fiori, 2017), tobacco stalks (Cai et al., 2016), citrus wastes (Erdogan et al., 2015) and wheat straw (Reza et al., 2015b) into solid biofuels with increased energy content. Upgrading via HTC is particularly suited to

biomasses with residues high in inorganic elements, *i.e.* to residues with a high ash mass fraction. Hydrothermal treatments, unlike dry thermochemical processes, can reduce the ash content of biomass and produce a solid hydrochar with coal-like properties that can be directly substituted in combustion systems (Kambo and Dutta, 2015; Reza et al., 2015a; Mäkelä et al., 2016; Mäkelä and Yoshikawa, 2016; Smith et al., 2016; Yang et al 2016).

Given the need to develop renewable fuels and to valorize marginal land, and the high moisture and ash content of *Opuntia ficus-indica*, the application of HTC technology to OC may represent a sustainable bio-energy generation pathway. This investigation analyzes the effects of HTC process variables (temperature, residence time and solid load) on the energy, thermal and chemical properties of the solid bio-fuel produced, including secondary char and mineral content. While the literature is replete with examples of the influence of temperature and residence time on hydrochar yield for a variety of biomasses, few studies probe the effect of solid loading on yield, a potentially important parameter to address the economical evaluation of the technology at industrial scale (Lucian and Fiori, 2017).

2. Material and methods

2.1. Materials and sample preparation

5 kg of *Opuntia ficus-indica* cladodes (OC) were collected from 2 to 3-year old prickly pear plants in the Palermo province of Sicily (Italy). The moisture content (as received) was 93 wt%. The fresh collected cladodes were cut into 10 mm squares and dried in a ventilated oven at 105 °C for 48 h. This pre-treatment was carried out to

prevent degradation of the feedstock before use, and to begin with a dry baseline. The samples were ground and sieved to a particle size between 300 and 850 μm. All samples were oven dried overnight at 105 °C before HTC tests, and the desired amount of water added immediately before each HTC run to the desired dry biomass to water ratio (B/W).

2.2. Hydrothermal carbonization of OC

HTC experiments were performed in a 50-mL stainless steel (AISI 316) batch reactor, designed and constructed in-house, as reported in previous studies (Fiori et al., 2014; Basso et al., 2015). For each experiment, the reactor was charged with 2.4 to 6.0 ± 0.001 g of dried sample and 20 to 34 ± 0.01 g of deionized water to obtain the desired B/W. The amount of sample and water was chosen in order to fully cover the feedstock with water and leave comparable free volumes in the system during experiments. Once the reactor was sealed, air was purged from the system by flushing with pure nitrogen (N_2, Airliquide Alphagaz 1^{TM}) three times. Nitrogen pressure was then lowered to ambient pressure, the valves upstream and downstream of the reactor were closed, the vessel was heated to the desired temperature, and held at this value for a desired residence time. The pressure reached in the various HTC runs was comprised in the range 13.5-60.2 bar and depended mostly on the run peak temperature.

Following this hold time, the reactor was rapidly quenched by placing it on a cold stainless steel disk at -24 °C while compressed air was blown into the reactor walls (quenching time less than 15 minutes). As the reactor reached room temperature, the

valve at the reactor outlet was opened to let the produced gases flow into a graduated cylinder filled with water. Gas mass yield was calculated from the gas volume by considering CO_2 as the sole gaseous reaction product. While gas composition varies, the typical CO_2 molar fraction in dry HTC gas is between 0.95 and 0.99, with minor amounts of CO and traces of H_2 and CH_4 (Hitzl et al., 2015; Basso et al., 2016). The reactor was then disassembled and the solid fraction was recovered by filtration. The solid residue was dried in a ventilated oven at 105 °C until constant weight (drying times longer than 3 hours).

Reaction temperature was set to either 180, 220 or 250 °C, for dry biomass to water ratios equal to 0.20, and then kept constant at 250 °C for experiments with varying B/W of 0.07, 0.14 and 0.30. Residence time was either 0.5, 1 or 3 h, performed at each temperature and solid load. This resulted in the production of 18 different hydrochars (described in Table 1), each of which was carried out at least in duplicate. Hydrochar yield (MY) was calculated as $MY = M_{HCdb} / M_{Rdb}$, where M_{HCdb} is the mass (dry basis) of the solid after thermal treatment (*i.e.*, hydrochar), and M_{Rdb} is the mass (dry basis) of the raw sample. Similarly, gas yield was defined as the mass of gas produced per unit mass of dry raw biomass sample. Liquid yield was calculated by difference.

2.3. Hydrochar characterization

Ultimate analyses were performed using a LECO 628 analyser equipped with Sulphur module for CHN (ASTM D-5373 standard method) and S (ASTM D-1552 standard method) content determination.

Proximate analyses were carried out by a LECO Thermogravimetric Analyser TGA 701 employing the ASTM D-3175-89 standard method: 20 °C/min ramp to 105 °C in air, held until constant weight (< ±0.05%) (moisture content); 16 °C/min ramp from 105 °C to 900 °C, hold time 7 min in N_2 (loss due to VM); isothermal hold at 800 °C in air (loss attributed to FC). Inorganic matter ("ash") comprised the residual. The parameter "hydrochar volatility" (V_{HC}) was here defined as $V_{HC} = VM/(1\text{-}ash)$ to express the quantity of "volatilizable" matter as a function of total "oxidizable" matter (comprising majority C, plus also H, N, and O).

The higher heating value (HHV) of solid samples was evaluated according to the CEN/TS 14918 standard by means of an IKA C 200 calorimeter. The energy yield (EY) of hydrochars was calculated as the hydrochar yield times the ratio of the HHV (dry basis) of the hydrochar and raw biomass, $EY = MY*HHV_{HCdb}/HHV_{Rdb}$.

To assess the surface functional groups of the resulting hydrochars, FTIR spectra of dried and ground raw material and hydrochars were obtained using a Perkin Elmer Spectrum 400 FT-IR/NIR spectrometer in mid-IR mode, equipped with a Universal ATR (attenuated total reflectance) sampling device containing a diamond/ZnSe crystal. An accessory plate with a conic awl was used which required only a few milligrams of sample without additional preparation. The pressure applied to squeeze the powdered sample towards the diamond was 130 ± 1 N.

SEM and EDS analysis was performed using a JEOL IT 300 scanning electron microscope and an EDS Bruker Quantax equipped with a SDDXFlash 630M detector. SEM analysis was carried out on selected samples to probe the impact of the severity of reaction conditions on morphology.

An analytical TGA (Mettler-Toledo TGA/DSC-1, 0.1 μg/0.1 °C resolution) was used to understand the impact of mineral matter on the thermal stability of the raw biomass versus the 250 °C, 3 h, B/W 0.20, "most severely carbonized" sample, alongside calcium oxalate monohydrate, identified via EDS as the primary mineral present (Fisher Scientific USA, minimum purity 98%). Between 6-9 mg of sample was placed in a 70 μL alumina crucible, dried at 110°C for 30 minutes under high purity nitrogen (min 99.99%, Airgas USA) and then heated at 5 °C/min up to 950°C, and held for 30 minutes. The DSC was calibrated with NIST-traceable indium and gold at 5 °C/min. These three samples were analyzed for the presence of crystalline phases by X-ray powder diffraction (XRD, Bruker D8 Discover) using Cu Ka radiation at 40 kV and 40 mA with a step size of 0.05 and dwell time of 0.5 s. Powder samples were affixed to the sample holder using Kapton tape, and a background Kapton tape spectrum taken at the same conditions was subtracted from all spectra.

3. Results and Discussion

The present work gauges the potential to transform *Opuntia ficus-indica* cladodes (OC), a draught-tolerant plant that can be grown on marginalized land, into a solid biomass fuel via hydrothermal carbonization. Using a large experimental matrix of 18 samples across mild to severe carbonization conditions, and applying ordinary least squares (OLS) linear regression analyses in both bivariate and multivariate cases (STATA v.13), enabled determination of the key process variables that dictate solid fuel quality and yield.

3.1. Effect of process variables on mass yields

The design of HTC processes requires knowledge of the overall solid yield of hydrochar produced as a function of reaction temperature, time, and biomass to water ratio. Fig. 1 reports the yield of solid, liquid and gas of OC HTC residues as a function of residence time, when varying the temperature (Fig. 1a) and the B/W (Fig. 1b). Data reported in Fig. 1 are the average of at least of two different trials with relative percentage errors (E_r%) lower than 1.7% for solid yields and lower than 2.2% for gas yields.

As shown in Fig. 1a, at constant B/W=0.20, the hydrochar yield was equal to 0.66 (T=180 °C, time=0.5 h) for mild conditions, and at the most severe conditions it decreased to 0.51 (T=250 °C, time=3 h). At this constant B/W loading, the relationship between hydrochar yield and temperature was highly linear with similar slopes, suggesting similar rates of biomass conversion. The observation that hydrochar yield decreased with increasing HTC temperature (all other variables constant) is well established in the literature; see for instance Benavente et al. (2015) and Mäkelä et al. (2015). The inverse relationship between reaction time and yield for OC is in agreement with the bulk of prior research; see for example Romàn et al. (2012), Basso et al. (2016) and Sabio et al. (2016), with contradicting results presented by Knezevic et al. (2010).

As shown in Fig. 1b, at a constant temperature of 250 °C, hydrochar yield varied between 0.42 (B/W=0.07, 3 h) and 0.63 (B/W=0.30, 0.5 h), overall increasing as B/W increased. These general trends are in agreement with previous results on HTC of olive waste (Volpe and Fiori, 2017) and woody biomass (Sermyagina et al. 2015). As

noted by Álvarez-Murillo et al. (2015) and Sabio et al. (2016) for HTC of olive stone and tomato-peel waste, in general an increase in B/W results in a slight increase in hydrochar yield, but such correlations between hydrochar yield and B/W did not hold across the range of operational conditions investigated. Likewise, Mäkelä et al. (2015) found no statistically significant effect of solid loading on multiple process outputs (including hydrochar yield) for HTC of lignocellulosic sludge. To date, the effect of solid loading on yield is not well established in the literature, and the available data are too scarce from which to generalize. For OC, the effect was extremely remarkable: moving from B/W=0.07 to B/W=0.30 resulted in an increase in hydrochar yield in the range 36-46%, depending on reaction time.

Gas yield increased both with temperature and residence time and solid load (Fig. 1a,b). At B/W=0.20, gas yield varied between 0.03 (T=180 °C, time=0.5 h) and 0.14 (T=250 °C, time=3 h). At 250 °C, gas yield varied between 0.07 (B/W=0.07, time=0.5 h) and 0.14 (B/W=0.20 and 0.30, time=3 h).

Liquid yield increased when increasing the temperature (Fig. 1a) and decreased when increasing solid load (Fig. 1b), while the effect of reaction time was almost negligible. Data reported in Fig. 1a testify that the higher the reaction temperature and time are, the larger the mass displaced from the solid to the liquid and gas phases. Gaseous molecules such as CO_2 and CO are generated directly from raw biomass via decarboxylation and decarbonylation reactions in the solid phase, and from the liquid phase where the organic molecules released from the biomass further decompose to CO_2 (Funke et al. 2010). Thus, the gas phase "receives" molecules from both the solid and liquid phases; in turn, its mass yield increased from 0.03 (at the lowest reaction

temperature and time) to 0.14 (at the highest reaction temperature and time). Conversely, the liquid phase receives mass from the solid phase and releases mass to the gas phase (and eventually back to the solid phase): liquid mass yield varied to a limited extent (0.30-0.37 – Fig. 1a), due to such partial counterbalancing of mass fluxes at varying HTC operating conditions.

Results reported in Fig. 1b allow a very interesting analysis. Different solid loads translate into different amounts of liquid water available as extracting medium: it is expected that increasing the amount of water increases the transfer of matter from solid to liquid phase. Going from B/W=0.30 to B/W=0.07 corresponds to about a four-fold increase in the amount of water per unit mass of feedstock: the liquid yield almost doubled (from 0.25 to 0.47) and, correspondingly, the concentration of dissolved organics in the liquid phase at B/W=0.07 was about half of that at B/W=0.30. At low B/W the liquid phase is more diluted in organics and, consequently, less reactive. This translates into a lower capacity to produce gaseous species: at low B/W, the gas yield was lower than at high B/W; and this could also affect the tendency of organics to polymerize into the liquid phase and precipitate back as a solid phase.

To capture the extent to which one process variable is more critical in determining yield (and other product parameters) than others, regression analyses were performed. Table 2 shows the results of bivariate and multivariate OLS linear regression analyses on the solid yield across all 18 samples. The bivariate (e.g. solid yield vs. temperature) regression suggests that temperature is indeed a highly statistically significant variable ($p < 0.01$) in determining yield, as noted above. As temperature

increases, the solid yield decreases (according to the regression) at a rate of 0.196 ± 0.054 % per °C. However, this linear model explains only 45% of the variation in the dependent variable (R^2 = 0.456). In the bivariate cases, time is not statistically significant. B/W is statistically significant, but with an R^2 of 0.609, this correlation explains only a slight majority of the variance in the data. This inability of a bivariate linear correlation using a single process variable to predict resulting solid yield is highlighted in Fig. 2a.

Therefore, we turn to multivariate linear analysis to consider the combined impacts of these process variables on yield. From Table 2, it is clear that the three variables (time, temperature, and B/W) are all statistically significant in determining the solid yield from HTC of OC, with the regression equation (Eq. 1) explaining over 96% of the variance of the data.

$$MY_{Char}\,(\%) = -0.168*Temp(°C) - 1.184*time(h) + 76.651*B/W(g/g) + 82.144 \quad (1)$$

Indeed, as shown in Fig. 2a, this correlation provides an excellent fit for the 18 samples produced at varying process conditions.

3.2. Hydrochar composition as a function of process variables

Ultimate analysis (Table 1) shows that HTC had little effect on the hydrogen content, which ranged between 4.6 and 4.9%. Hydrochars showed a small increase in nitrogen compared to the raw material; the nitrogen content does not show any clear dependence on HTC process variables. A negligible amount of sulphur (0.01-0.15%, data not reported) was detected for both raw biomass and hydrochars.

Carbon content increased with the increase in temperature and when the reaction time increased from 0.5 to 1 h. Carbon contents at residence times of 1 and 3 h were quite similar. Oxygen content had an opposite trend compared to that of carbon. The multivariate OLS regression, shown in Table 3, confirms that reaction temperature is statistically significant ($p<0.05$) in increasing C content, while decreasing both time and temperature lead to increases in O content. However, this linear regression explains only 46 and 45% of the variance of the data, respectively.

Overall, as HTC temperature and residence time increased, the fixed carbon content (FC) increased, and the volatile matter (VM) content decreased, as shown in Table 1. And in fact, a multivariate linear regression considering temperature, time and B/W confirms that temperature and time are statistically significant in describing the VM and FC contents resulting from carbonization, though only with correlation coefficients of 0.725 and 0.657, respectively (Table 3).

When compared to the raw biomass, the inorganic (ash) content decreased by ~2.0-2.5% in absolute terms for low-temperature (180 and 220 °C) and short residence time (0.5 h) hydrochars, while it remained approximately constant (± 1%) for samples carbonized at 250 °C with a reaction time of 1-3 h. During hydrothermal treatments inorganic elements (in particular Na^+ and K^+) are removed from the solid phase, even at less severe process conditions (Reza et al., 2015a). At longer residence times and higher temperatures, the organic mass depletion compensates for the inorganic element loss, resulting in an approximately constant “ash” mass fraction.

3.3. Impact of processing on hydrochar energy properties and char formation

Table 1 shows the HHV and the EY of the hydrochars obtained at the different operating conditions. As expected, at fixed B/W=0.20, the hydrochars' HHVs increase with increasing HTC temperature and residence time (Fig. 3a). The highest HHV is seen for the hydrochar obtained at 250 °C and 3 h of residence time: 22.4 MJ kg^{-1}, 1.6 times greater than the HHV of the raw feedstock.

As shown in Table 1, for samples carbonized at B/W=0.20 the energy yield is rather uniform and ranges from 0.78 to 0.84, without any obvious trends between EY and process variables. This behavior results from the counterbalancing effects of the process variables reaction temperature and time on hydrochar yield and HHV. Notably, EY does vary significantly with B/W; it is at a maximum for the highest B/W (EY=0.92) and minimum for the lowest B/W (EY=0.63). These observations are underscored by the regression results in Table 2; in a multivariate regression, only B/W is statistically significant; Eq. (2) was able to explain 95% of the variance within the energy yield as a function of process parameters (see Fig. 2b for measured vs predicted plot).

$$EY\ (\%) = -0.017*Temp(°C) + 0.195*time(h) + 123.521*B/W(g/g) + 59.816 \quad (2)$$

If the HTC process goal is to maximize EY, this suggests working at higher values of B/W, which would also maximize the profitability of an industrial HTC plant by enabling higher throughput (Lucian and Fiori, 2017).

Fig. 3 shows the behaviour of HHV and "hydrochar volatility" V_{HC} obtained at fixed B/W (Fig. 3a,b) and fixed temperature (Fig. 3c,d) when varying the other operating conditions.

The HHV increase with temperature follows a linear trend (Fig. 3a). V_{HC} increases together with hydrochar yield (Fig. 3b): at the less severe operating conditions, higher mass yields and more volatile hydrochars are obtained.

The comparison of the behaviour of HHV vs. hydrochar yield outlined by Fig.s 3b and c is of particular interest. The inverse proportionality of HHV to hydrochar yield, well documented in the HTC literature (Basso et al., 2015; Sermyagina et al., 2015), applies only when working at variable reaction temperature and time, but at fixed B/W. If B/W also varies, such a correlation is no longer valid: correlating linearly all the HHV and yield data of Fig. 3c returns a R^2=0.0005. Conversely, the linear relationship between HHV and yield holds when considering the subgroups of data obtained at fixed B/W: this strictly applies for B/W equal to 0.07, 0.20 and 0.30 ($0.97 \leq R^2 \leq 1$), while is less evident for B/W=0.14 (R^2=0.61). Such a behaviour is emphasized by the bivariate analysis used to predict HHV as a function of solid yield, which describes less than 35% of the variance in the data, as shown in Table 2 (and graphically in Fig. 2c). Temperature is the only single process variable that can describe a majority of the variance of the data (R^2=0.738) in a bivariate analysis (HHV vs temperature). In the multivariable linear analysis (regression including time, temperature, and B/W; inclusion of solid yield, given its dependence on these variables, would introduce collinearity issues) only temperature and time are statistically significant. This results in a regression equation of:

$$HHV\ (MJ/kg) = 0.051*Temp(°C) + 0.508*time(h) + 2.726*B/W(g/g) + 6.798 \quad (3)$$

whose outputs are shown graphically in Fig. 2c.

While the coefficient for B/W is larger (2.726), its error is of equal weight (2.016). However, this does not mean that B/W is not a critically important factor in HTC of biomass, rather, it is not linearly correlated with HHV. Fig. 3d highlights that the HHV behaviour vs. B/W yields a maximum. Starting from B/W=0.07, HHV first increases, is maximized at B/W equal to 0.14 or 0.20 (depending on residence time), then decreases at B/W=0.30. This trend appears to be inversely correlated to the hydrochar volatility. V_{HC} appears relatively stable for B/W=0.07 and B/W=0.14, then it drops down at B/W=0.20, and increases again at B/W=0.30. V_{HC} values obtained at reaction times of 0.5 and 1 h are quite similar, while increasing the duration of HTC decreases the volatile matter present.

SEM images shed light on the morphological changes due to HTC. Fig. 4 shows a series of SEM images for OC that underwent increasingly severe carbonization. Fig. 4a shows how at 180 °C (3 h, B/W=0.20) the HTC conditions were not sufficient to destroy the fibrous nature of the biomass; intact OC fibers abound in the low temperature samples. Given the low HHV, high solid yield and VM of these samples, the lack of complete fiber decomposition is not surprising. The impact of reaction time on surface morphology can be seen in Fig.s 4b (for 250 °C, 0.5 h, B/W=0.20 char) and 4c,d (250 °C, 3 h, B/W=0.20 char). As the carbonization time increases, there is a distinct transition from a char with some fibrous nature to a more amorphous solid with spherical carbon deposits, which are likely linked to secondary char formation.

The solid residue resulting from HTC processes can be either primary char or secondary char (Knezevic et al., 2010). The former results from solid-solid

conversion: the primary char maintains the original shape of the raw biomass, representing the non-liquefied remainder of the biomass. The latter, sometimes referred to as coke (Karayildirim et al., 2008), results from the polymerization of biomass degradation products, such as HMF and furfural. Secondary char formation pathways proceed via hydrolysis, dissolution, polymerization, aromatization, and condensation to produce spherical carbonized particles (Karayildirim et al., 2008; Knezevic et al., 2010; Titirici et al., 2008; Titirici et al., 2012; Castello et al., 2014). Recent results from this laboratory on the HTC of olive waste demonstrated that secondary char is richer in carbon than primary char, and higher amounts of secondary char are often seen for chars with high HHV and FC content (Volpe and Fiori, 2017).

To probe the characteristics of the primary char structure, the 250 °C, 3 h, B/W=0.20 sample was washed repeatedly with at 50:50 methanol:acetone mixture (until the solution ran clear) to dissolve the secondary char. SEM images of the solid residue after washing show a crater-filled landscape, dotted with "pockets" that were originally covered by the spherical secondary char particles (Fig.s 4 e,f). The "hole" sizes of these craters are similar in diameter to the spherical particles (measurements shown in SI).

The data of Fig. 3 and the SEM images testify the importance (very often neglected in the HTC literature) of B/W on HTC reactions, in terms of degree of carbonization and, more importantly, secondary char formation. The 250 °C, 3 h, B/W=0.07 sample shows some evidence of secondary char formation with amorphous carbon regions, but the spherical nature of the secondary char is not nearly as developed as in the

samples with B/W of 0.20 and 0.30 (additional images available in SI). At low B/W (B/W=0.07), the aqueous phase is diluted in organics (Section 3.1) which limits their polymerization and back precipitation to the solid phase. At higher B/W there is substantial concentration of species like HMF and furfural which can later polymerize, producing secondary char. The differences in HHV and V_{HC} between the samples obtained at B/W of 0.20 and 0.30 (Fig. 3d) could be because biomass hydrolysed to a lower extent due to the limited availability of water in the case of higher B/W, this overall limiting the carbonization degree which was maximized at B/W=0.20 and prolonged residence times.

Future work will probe the aqueous and solid phase composition (especially concentrations of HMF and furfural) in conjunction with qualitative observations of the hydrochar samples.

3.4. Inorganic content of hydrochars

In addition to the two carbonaceous phases brought to light via SEM imaging, the nature of the inorganic ("ash") content was also revealed. As shown in Fig. 4f, SEM images showed crystalline structures separate from the char particles. EDS analysis suggested a composition of 1 atom of calcium per ~2 carbon and ~4 oxygen, suggesting that the crystalline material may be calcium oxalate, CaC_2O_4. XRD analysis confirmed the presence of CaC_2O_4 in the HTC char (signal too weak to detect in raw biomass; XRD patterns available in SI). Notably, primary peaks for $CaC_2O_4 \bullet H_2O$ at 2θ = 28 (020); 30.5 (202), 31.0 (121); 31.2 (310); 36.5 (301); 37.2 (130) and 40.8 (202) were detected (Girija et al. 1998).

TGA analysis of the raw OC, HTC 250 °C, 3 h, B/W=0.20 sample, and pure $CaC_2O_4 \bullet H_2O$ suggests that calcium oxalate is indeed a primary constituent of the hydrochar's inorganic components. Calcium oxalate (monohydrate) undergoes three thermal decomposition reactions in an inert atmosphere (Fig. 5a):

Loss of hydrated water: $CaC_2O_4 \bullet H_2O \rightarrow CaC_2O_4 + H_2O$

Decomposition to calcium carbonate: $CaC_2O_4 \rightarrow CaCO_3 + CO$

Decomposition to calcium oxide: $CaCO_3 \rightarrow CaO + CO_2$

Derivative thermogravimetric (DTG) curves of $CaC_2O_4 \bullet H_2O$ show three peaks, corresponding to each decomposition phase. Theoretically, 12.3% of the mass will be lost during the first decomposition reaction, 19.2% during the second, and 30.1% during the third. This was indeed observed for pure $CaC_2O_4 \bullet H_2O$ (Fig. 5b and SI). Furthermore, in Fig. 5, the raw and carbonized biomasses showed evidence of calcium oxalate present, with peak mass loss rates occurring at similar temperatures to the decomposition reactions (Fig. 5b). It also appears that the hydrochar had a higher concentration of $CaC_2O_4 \bullet H_2O$ (expected given above discussion concerning removal of inorganics and depletion of organics during HTC); the thermogravimetric (TG; mass fraction lost) curves show that the raw biomass pyrolyzes fairly continuously across the temperature range, with DTG peaks occurring at the same temperatures as for $CaC_2O_4 \bullet H_2O$. However, the hydrochar TG and DTG curves more closely mimic that of the calcium oxalate. One cannot overlook, however, the difference in DSC curves (Fig. 5c); while the $CaC_2O_4 \bullet H_2O$ curve is entirely endothermic, as would be expected for a thermal decomposition reaction, both the raw and hydrochar are exothermic at temperatures greater than ~500 °C, and actually

peak at the same temperature of the $CaCO_3 \rightarrow CaO + CO_2$ decomposition reaction. We suspect, and future work will explore this concept further, that the release of CO_2 from the calcium carbonate may gasify the chars. Such CO_2 biomass gasification reactions are exothermic, and CaO has a known capacity to adsorb CO_2 (Acharya et al., 2009). It is plausible that a considerable amount of CO_2 was available to react with the biomass/hydrochar, resulting in the observed exothermic behavior; the higher concentration of $CaC_2O_4 \bullet H_2O$ in the hydrochar supports the finding of a more exothermic reaction for the hydrochar vs. raw sample.

3.5. Surface characteristics of hydrochars

ATR-FTIR spectroscopy was used to assess the surface functional group changes in *Opuntia Indica cladodes* resulting from carbonization, as shown in Fig. 6. FTIR peak assignments were made according to Xu et al. (2013). While strong single bond vibrations typical of lignocellulosic biomass that contains cellulose, hemicelluloses and lignin, such as C-O, C-H and O-H, are still present in carbonized samples, significant decreases were observed at increasing HTC temperature (Fig. 6a) and, although with less intensity, at increasing residence time (Fig. 6b).

The broad peak between 3600 and 3000 cm^{-1} is attributed to the stretching vibration of aliphatic O-H (hydroxyl, phenols and carboxyl); the peaks between 1100 and 1000 cm^{-1} correspond to C-O stretching vibration from esters, phenols and aliphatic alcohols while the peak at 1200 cm^{-1} is assigned to the O-H bending mode. The lower intensity of these peaks in the hydrochars suggests that dehydration (weakening of bands at 3600-3000 cm^{-1} due to O-H stretching and at 1200 cm^{-1} due to O-H bending)

and decarboxylation reactions (disappearing of bands at 1100-1000 cm^{-1}) occurred during HTC (Parshetti et al., 2013).

The peak between 1700 and 1650 cm^{-1} corresponds to the C-O stretching vibration of esters, carboxylic acids or aldehydes from cellulose or lignin, while the peak between 1650 and 1450 cm^{-1} represents the C=C vibrations of the aromatic rings in lignin. These peaks demonstrate considerable changes in the hydrochars due to the breakdown of cellulose and aromatic rings (lignin partial fragmentation) during HTC (Liu et al., 2013). The peaks between 2940 and 2840 cm^{-1} and 1450 and 1200 cm^{-1} are due to the stretching and bending vibration of aliphatic C-H bonds, respectively. The presence of such typical bands in hydrochar FTIR spectra indicates that aliphatic structures are maintained in hydrochars. The appearance, with increasing HTC temperature, of a shoulder around 2950-2970 cm^{-1}, and the peaks at 825 and 660 (C-H aromatic vibrations) suggest an increase in aromatic character during carbonization. The progressive decrease in intensity, with increasing HTC temperature, of the bands between 930 and 875 cm^{-1}, assigned to the glycosidic linkage of hemicellulose and cellulose, clearly attests the breakage of such bonds during carbonization. Similar chemical transformations, with hemicellulose and cellulose destruction and increasing aromatization, were observed using FTIR when corncob and miscanthus were converted into carbonaceous products by means of HTC (Calucci et al., 2013).

4. Conclusions

Hydrothermal carbonization was demonstrated as a potential technology to convert high-moisture *Opuntia ficus-indica* cladodes, a biomass cultivable on arid and marginal lands, into a sustainable solid biofuel. Using multivariate statistical analysis, it was shown that hydrochar yield, energy content, composition, surface chemistry and morphology, depend, to varying degrees, on carbonization temperature, reaction time, and solid loading. Electron microscopy showed evidence of secondary char formation at higher temperatures and residence times. Crystallographic and thermal analyses suggest calcium oxalate, present in biomass, concentrates in char, and may promote gasification at high temperature.

Acknowledgements

The authors thank L. Gao for assistance with running TGA. This work was partially supported by the U.S.-Italy Fulbright Commission.

Appendix A. Supplementary information

Supplementary data associated with this article can be found in "Supplementary information".

References

1. Álvarez-Murillo, A., Román, S., Ledesma, B., Sabio, E., 2015. Study of variables in energy densification of olive stone by hydrothermal carbonization. J. Anal. Appl. Pyrolysis 113, 307–314. doi:10.1016/j.jaap.2015.01.031
2. Archarya, B., Dutta, A., Basu, P. 2009. Chemical-looping gasification of biomass for hydrogen-enriched gas production with in-process carbon dioxide capture. Energy Fuels. 23, 5077-5083. doi: 10.1021/ef9003889
3. Basso, D., Weiss-Hortala, E., Patuzzi, F., Castello, D., Baratieri, M., Fiori, L., 2015. Hydrothermal carbonization of off-specification compost: A byproduct of

the organic municipal solid waste treatment. Bioresour. Technol. 182, 217-224. doi:10.1016/j.biortech.2015.01.118
4. Basso, D., Patuzzi, F., Castello, D., Baratieri, M., Rada, E.C., Weiss-Hortala, E., Fiori, L., 2016. Agro-industrial waste to solid biofuel through hydrothermal carbonization. Waste Manag. 47, 114–121. doi:10.1016/j.wasman.2015.05.013
5. Benavente, V., Calabuig, E., Fullana, A., 2015. Upgrading of moist agro-industrial wastes by hydrothermal carbonization. J. Anal. Appl. Pyrolysis 113, 89-98. doi:10.1016/j.jaap.2014.11.004
6. Cai, J., Li, B., Chen, C., Wang, J., Zhao, M., Zhang, K., 2016. Hydrothermal carbonization of tobacco stalk for fuel application. Bioresour. Technol. 220, 305–311. doi:10.1016/j.biortech.2016.08.098
7. Calucci, L., Rasse, D.P., Forte, C., 2013. Solid-state nuclear magnetic resonance characterization of chars obtained from hydrothermal carbonization of corncob and Miscanthus. Energy and Fuels 27, 303–309. doi:10.1021/ef3017128
8. Castello, D., Kruse, A., Fiori, L., 2014. Supercritical water gasification of hydrochar, Chem. Eng. Res. Des. 92, 1864–1875. doi:10.1016/j.cherd.2014.05.024.
9. Corneli, E., Dragoni, F., Adessi, A., De Philippis, R., Bonari, E., Ragaglini, G., 2016. Energy conversion of biomass crops and agroindustrial residues by combined biohydrogen / biomethane system and anaerobic digestion. Bioresour. Technol. 211, 509–518. doi:10.1016/j.biortech.2016.03.134
10. Erdogan, E., Atila, B., Mumme, J., Reza, M.T., Toptas, A., Elibol, M., Yanik, J., 2015. Characterization of products from hydrothermal carbonization of orange pomace including anaerobic digestibility of process liquor. Bioresour. Technol. 196, 35–42. doi:10.1016/j.biortech.2015.06.115
11. Fiori, L., Basso, D., Castello, D., Baratieri, M., 2014. Hydrothermal carbonization of biomass: Design of a batch reactor and preliminary experimental results. Chem. Eng. Trans. 37, 55–60. doi:10.3303/CET1437010
12. Funke, A., Ziegler, F. 2010. Hydrothermal carbonization of biomass: A summary and discussion of chemical mechnaisms for process engineering. Biofuels, Bioprod. Biorefin. doi: 10.1022/bbb.198
13. Girija, E.K., Latha, S.C., Kalkura, S.N., Subramanian, C., Ramasamy, P. 1998. Crystallization and microhardness of calcium oxalate monohydrate. Mater. Chem. Phys. 52, 253-257. doi: 10.1016/S0254-0584(97)02053-1
14. Hitzl, M., Corma, A., Pomares, F., Renz, M., 2015. The hydrothermal carbonization (HTC) plant as a decentral biorefinery for wet biomass. Catal. Today 257, 154–159. doi:10.1016/j.cattod.2014.09.024
15. ISTAT, 2016. Produzione agricola totale per tipo di prodotto e anno (quintali) [web document]. http://www.istat.it/it/sicilia/dati?qt=gettable&dataset=DCSP_COLTIVAZ&dim=120,3,9,0,0&lang=2&tr=0&te=0 (accessed 23.02.17).
16. Kambo, H.S., Dutta, A., 2015. Comparative evaluation of torrefaction and hydrothermal carbonization of lignocellulosic biomass for the production of solid biofuel. Energy Convers. Manag. 105, 746–755. doi:10.1016/j.enconman.2015.08.031

17. Karayıldırım, T., Sınağ, A., Kruse, A., 2008. Char and coke formation as unwanted side reaction of the hydrothermal biomass gasification. Chem. Eng. Technol. 31, 1561–1568. doi:10.1002/ceat.200800278
18. Knežević, D., van Swaaij, W., Kersten, S., 2010. Hydrothermal conversion of biomass. II. Conversion of wood, pyrolysis oil, and glucose in hot compressed water. Ind. Eng. Chem. Res. 49, 104–112. doi:10.1021/ie900964u
19. Liu, Z., Quek, A., Hoekman, S.K., Balasubramanian, R., 2013. Production of solid biochar fuel from waste biomass by hydrothermal carbonization. Fuel 103, 943–949. doi:10.1016/j.fuel.2012.07.069
20. Lucian, M., Fiori, L., 2017. Hydrothermal carbonization of waste biomass: Process design, modeling, energy efficiency and cost analysis. Energies 10, 211. doi:10.3390/en10020211
21. Mäkelä, M., Benavente, V., Fullana, A., 2015. Hydrothermal carbonization of lignocellulosic biomass: Effect of process conditions on hydrochar properties. Appl. Energy 155, 576–584. doi:10.1016/j.apenergy.2015.06.022
22. Mäkelä, M., Fullana, A., Yoshikawa, K., 2016. Ash behavior during hydrothermal treatment for solid fuel applications. Part 1: Overview of different feedstock. Energy Convers. Manag. 121, 402-408. doi:10.1016/j.enconman.2016.05.016
23. Mäkelä, M., Yoshikawa, K., 2016. Ash behavior during hydrothermal treatment for solid fuel applications. Part 2: Effects of treatment conditions on industrial waste biomass. Energy Convers. Manag. 121, 409-414. doi:10.1016/j.enconman.2016.05.015
24. Onakpoya, I.J., O'Sullivan, J., Heneghan, C.J., 2015. The effect of cactus pear (*Opuntia ficus-indica*) on body weight and cardiovascular risk factors: a systematic review and meta-analysis of randomized clinical trials. Nutrition 31, 640–646. doi:10.1016/j.nut.2014.11.015
25. Pala, M., Kantarli, I.C., Buyukisik, H.B., Yanik, J., 2014. Hydrothermal carbonization and torrefaction of grape pomace : A comparative evaluation. Bioresour. Technol. 161, 255–262. doi:10.1016/j.biortech.2014.03.052
26. Parshetti, G.K., Hoekman, S.K., Balasubramanian, R., 2013. Chemical, structural and combustion characteristics of carbonaceous products obtained by hydrothermal carbonization of palm empty fruit bunches. Bioresour. Technol. 135, 683-689. doi:10.1016/j.biortech.2012.09.042
27. Reza, M.T., Lynam, J.G., Uddin, M.H, Coronella, C.J., 2013. Hydrothermal carbonization: Fate of inorganics. Biomass Bioenergy 49, 86–94. doi:10.1016/j.biombioe.2012.12.004
28. Reza, M.T., Emerson, R., Uddin, M.H., Gresham, G., Coronella, C.J., 2015a. Ash reduction of corn stover by mild hydrothermal preprocessing. Biomass Convers. Biorefinery 5, 21–31. doi:10.1007/s13399-014-0122-x
29. Reza, M.T., Rottler, E., Herklotz, L., Wirth, B., 2015b. Hydrothermal carbonization (HTC) of wheat straw: influence of feedwater pH prepared by acetic acid and potassium hydroxide. Bioresour. Technol. 182, 336–344. doi:10.1016/j.biortech.2015.02.024
30. Román, S., Nabais, J.M.V., Laginhas, C., Ledesma, B., González, J.F., 2012,

Hydrothermal carbonization as an effective way of densifying the energy content of biomass, Fuel Process. Technol. 103, 78–83. doi:10.1016/j.fuproc.2011.11.009
31. Sabio, E., Álvarez-Murillo, A., Román, S., Ledesma, B., 2016. Conversion of tomato-peel waste into solid fuel by hydrothermal carbonization: Influence of the processing variables. Waste Manag. 47, 122–132. doi:10.1016/j.wasman.2015.04.016
32. Santos, T. do N., Dutra, E.D., Gomes do Prado, A., Leite, F.C.B., de Souza, R. de F.R., dos Santos, D.C., Moraes de Abreu, C.A., Simões, D.A., de Morais, M.A., Menezes, R.S.C., 2016. Potential for biofuels from the biomass of prickly pear cladodes: Challenges for bioethanol and biogas production in dry areas. Biomass Bioenergy 85, 215–222. doi:10.1016/j.biombioe.2015.12.005
33. Sermyagina, E., Saari, J., Kaikko, J., Vakkilainen, E., 2015. Hydrothermal carbonization of coniferous biomass: Effect of process parameters on mass and energy yields. J. Anal. Appl. Pyrolysis 113, 551–556. doi:10.1016/j.jaap.2015.03.012
34. Smith, A.M., Singh, S., Ross, A.B., 2016. Fate of inorganic material during hydrothermal carbonisation of biomass: Influence of feedstock on combustion behaviour of hydrochar. Fuel 169, 135–145. doi:10.1016/j.fuel.2015.12.006
35. Titirici, M-M., Antonietti, M., Baccile, N., 2008. Hydrothermal carbon from biomass: a comparison of the local structure from poly- to monosaccharides and pentoses/hexoses. Green Chem. 10, 1204-1212. doi:10.1039/b807009a
36. Titirici, M.-M., White, R.J., Falco, C., Sevilla, M., 2012. Black perspectives for a green future: hydrothermal carbons for environment protection and energy storage. Energy Environ. Sci. 5. 6796–6822. doi:10.1039/c2ee21166a
37. Volpe, M., D'anna, C., Messineo, S., Volpe, R., Messineo, A., 2014. Sustainable Production of Bio-Combustibles from Pyrolysis of Agro-Industrial Wastes. Sustainability 6, 7866–7882. doi:10.3390/su6117866
38. Volpe, M., Fiori, L., 2017. From olive waste to solid biofuel through hydrothermalcarbonisation: the role of temperature and solid load on secondarychar formation and hydrochar energy properties. J. Anal. Appl. Pyrolysis. 124, 63-72. doi:10.1016/j.jaap.2017.02.022
39. Volpe, M., Fiori, L., Volpe, R., Messineo, A., 2016. Upgrading of Olive Tree Trimmings Residue as Biofuel by Hydrothermal Carbonization and Torrefaction: A Comparative Study. Chem. Eng. Trans. 50, 13–18. doi:10.3303/CET1650003
40. Wikberg, H., Ohra-aho, T., Honkanen, M., Kanerva, H., Harlin, A., Vippola, M., Laine, C., 2016. Hydrothermal carbonization of pulp mill streams. Bioresour. Technol. 212, 236–244. doi:10.1016/j.biortech.2016.04.061
41. Xu, F., Yu, J., Tesso, T., Dowell, F., Wang, D., 2013. Qualitative and quantitative analysis of lignocellulosic biomass using infrared techniques: A mini-review. Appl. Energy 104, 801–809. doi:10.1016/j.apenergy.2012.12.019
42. Yang, L., Lu, M., Carl, S., Mayer, J.A., Cushman, J.C., Tian, E., Lin, H., 2015. Biomass characterization of *Agave* and *Opuntia* as potential biofuel feedstocks. Biomass Bioenergy 76, 43–53. doi:10.1016/j.biombioe.2015.03.004

43. Yang, W., Wang, H., Zhang, M., Zhu, J., Zhou, J., Wu, S., 2016. Fuel properties and combustion kinetics of hydrochar prepared by hydrothermal carbonization of bamboo. Bioresour. Technol. 205, 199–204. doi:10.1016/j.biortech.2016.01.068

Table 1. Process parameters and resulting properties of solid residues. Compositional analyses performed in duplicate; average values shown (Er% ≤ 3.3% for proximate and 1.0% for ultimate analyses); HHVs average of three measurements, Er%≤ 1.0)

Sample description				Proximate analysis			Elemental analysis				Energy properties	
Sample	**T (°C)**	**Time (h)**	**B/W**	**VM**	**FC**	**Ash**	**C**	**H**	**N**	**O***	**HHV (MJ kg^{-1})**	**EY**
	Raw			70.62	14.23	15.15	39.68	4.70	0.48	39.98	13.87	1
180_0.5_20	180	0.5	0.20	71.36	16.22	12.42	44.82	4.91	0.75	37.11	16.80	0.80
180_1_20	180	1.0	0.20	68.96	16.92	14.12	49.38	4.71	0.72	31.07	17.31	0.81
180_3_20	180	3.0	0.20	67.00	18.39	14.61	50.23	4.63	0.77	27.74	17.93	0.83
220_0.5_20	220	0.5	0.20	67.14	19.69	13.17	46.20	4.59	0.80	35.24	18.82	0.84
220_1_20	220	1.0	0.20	64.57	20.26	15.17	51.29	4.72	0.84	27.98	18.93	0.81
220_3_20	220	3.0	0.20	64.23	20.81	14.96	50.32	4.90	0.77	29.05	19.48	0.83
250_0.5_20	250	0.5	0.20	63.89	22.07	14.04	47.47	4.61	0.77	33.11	20.34	0.78
250_1_20	250	1.0	0.20	60.83	24.98	14.19	52.86	4.81	0.89	27.25	21.03	0.80
250_3_20	250	3.0	0.20	56.88	28.17	14.95	50.48	4.83	0.81	28.94	22.39	0.83
250_0.5_30	250	0.5	0.30	64.04	19.53	16.43	49.02	4.62	0.87	28.29	20.12	0.92
250_1_30	250	1.0	0.30	61.86	21.73	16.41	52.53	4.65	1.03	23.99	20.90	0.92
250_3_30	250	3.0	0.30	63.20	21.53	15.27	50.91	4.70	0.97	26.23	21.07	0.92
250_0.5_14	250	0.5	0.14	65.77	19.91	14.32	50.52	4.83	0.78	29.55	20.76	0.79
250_1_14	250	1.0	0.14	65.94	19.92	14.13	51.08	4.88	0.84	29.07	20.96	0.72
250_3_14	250	3.0	0.14	63.32	22.85	13.84	53.08	4.77	0.95	27.35	22.31	0.73
250_0.5_7	250	0.5	0.07	66.33	20.63	13.04	49.64	4.88	0.75	31.69	19.17	0.64
250_1_7	250	1.0	0.07	65.21	20.66	14.13	53.95	4.74	0.91	26.28	19.53	0.63
250_3_7	250	3.0	0.07	60.61	24.69	14.69	52.77	4.69	1.03	26.81	20.82	0.63

(VM = volatile matter, FC = fixed carbon, Ash = ashes; all dry basis),* calculated by difference.

Table 2. Results of OLS linear regression (bivariate and multivariate) to determine impact of process variables on solid yield and energy content of hydrochars

	Bivariate OLS Regressions				Multivariate
Impact of process variables on hydrochar yield					
Temperature	-0.196**				-0.168**
°C	(0.054)				(0.014)
Time		-1.184			-1.184**
h		(1.739)			(0.346)
B/W			85.304**		76.651**
			(17.089)		(5.409)
Constant	101.040**	57.090**	39.533**		82.144**
	(12.572)	(3.214)	(3.378)		(3.683)
R-squared	0.456	0.028	0.609		0.966
Impact of process variables on energy yield (EY)					
Temperature	-0.062				-0.017
°C	(0.083)				(0.021)
Time		0.195			0.195
h		(2.062)			(0.495)
B/W			124.397**		123.521**
			(7.387)		(7.743)
Solid Yield				0.947**	
%				(0.172)	
Constant	93.420**	78.696**	55.975**	26.604*	59.816**
	(19.598)	(3.812)	(1.460)	(9.582)	(5.271)
R-squared	0.033	0.001	0.947	0.656	0.950
Impact of process variables on higher heating value (HHV)					
Temperature	0.050**				0.051**
°C	(0.007)				(0.005)
Time		0.508			0.508**
h		(0.329)			(0.129)
B/W			0.110		2.726
			(5.462)		(2.016)
Solid Yield				-0.117*	
%				(0.040)	
Constant	8.295**	19.165**	19.906**	26.420**	6.798**
	(1.743)	(0.608)	(1.080)	(2.258)	(1.373)
R-squared	0.738	0.130	0.000	0.345	0.883
Observations	18	18	18	18	18
Standard errors in parentheses				** p<0.01, * p<0.05	

Table 3. Results of OLS multivariate linear regression to determine impact of process variables on hydrochar composition

Multivariate regressions to determine impact of process parameters on		
	Elemental C	*Elemental O*
Temperature	0.043*	-0.060*
°C	(-0.018)	(0.024)
Time	0.88	-1.363*
h	(-0.424)	(0.588)
B/W	-6.507	-7.954
	(-6.631)	(9.201)
Constant	40.172**	46.689**
	(-4.514)	(6.264)
R-squared	0.463	0.453
	Volatile Matter (VM)	*Fixed Carbon (FC)*
Temperature	-0.087**	0.071**
°C	(0.017)	(0.017)
Time	-1.398**	1.161*
h	(0.416)	(0.404)
B/W	-8.518	-0.620
	(6.508)	(6.316)
Constant	88.439**	2.806
	(4.431)	(4.300)
R-squared	0.725	0.657
Observations	18	18
Standard errors in parentheses		** p<0.01, * p<0.05

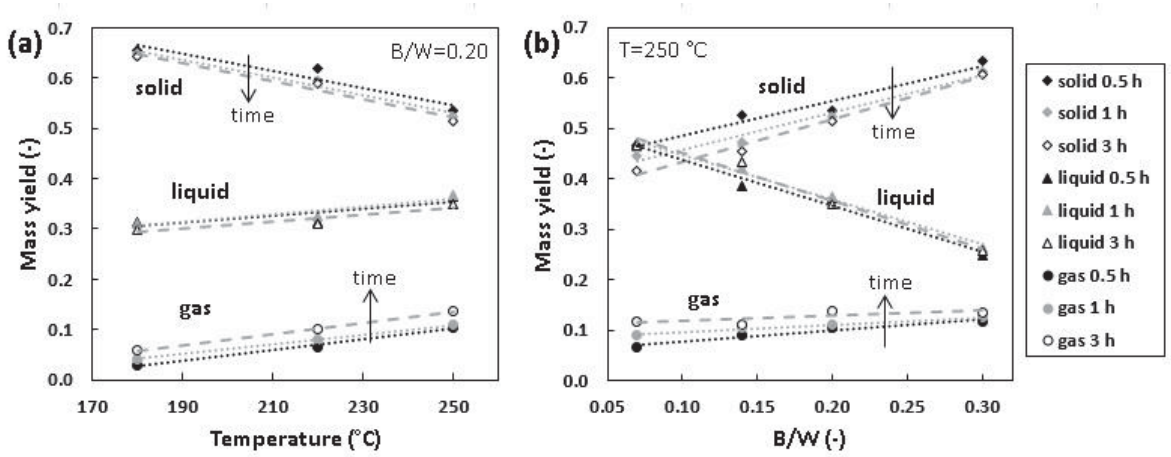

Fig. 1. HTC mass balance. Mass yield of solid, gas and liquid (by difference); (a) at different temperatures and reaction times (B/W=0.20); (b) at different biomass loads and reaction times (T=250 °C). Black closed indicators: 0.5 h; grey closed indicators: 1 h; open indicators: 3 h. Straight lines represent the linear fitting of the data and help in reading the graph.

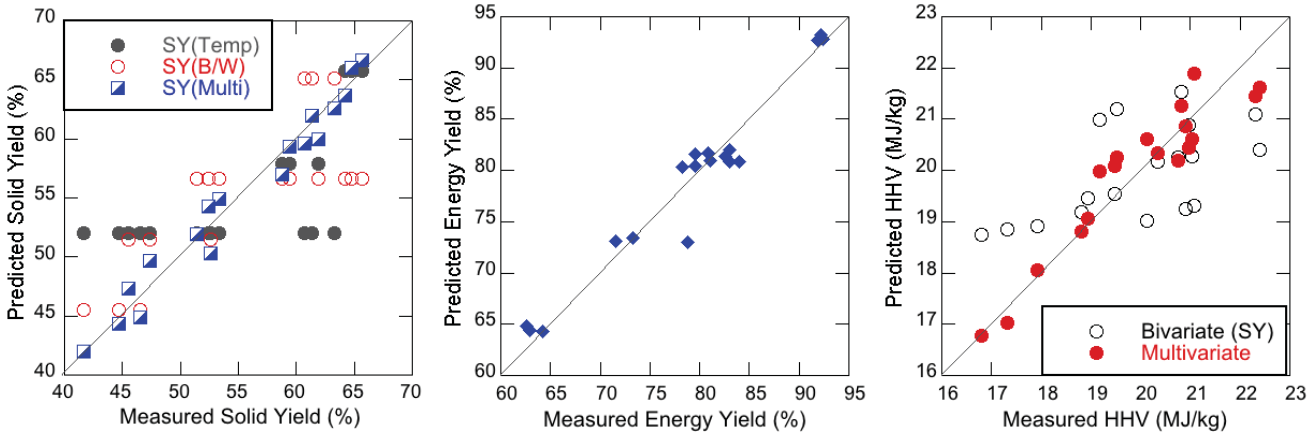

a. Predicted (bivariate) versus actual solid yield as a function of temperature (closed circle) or B/W (open circle); and Predicted (multivariate OLS regression, Eq. (1)) (half filled square) versus actual solid yield, with y=x line

b. Predicted (multivariate OLS regression, Eq. (2)) versus measured energy yield, with y=x line

c. Predicted (bivariate with only solid yield; multivariate with time, temperature, B/W, Eq. (3)) versus measured HHV, with y=x line

Fig. 2. Predicted versus measured hydrochar yield (a), energy yield (b), higher heating value (c).

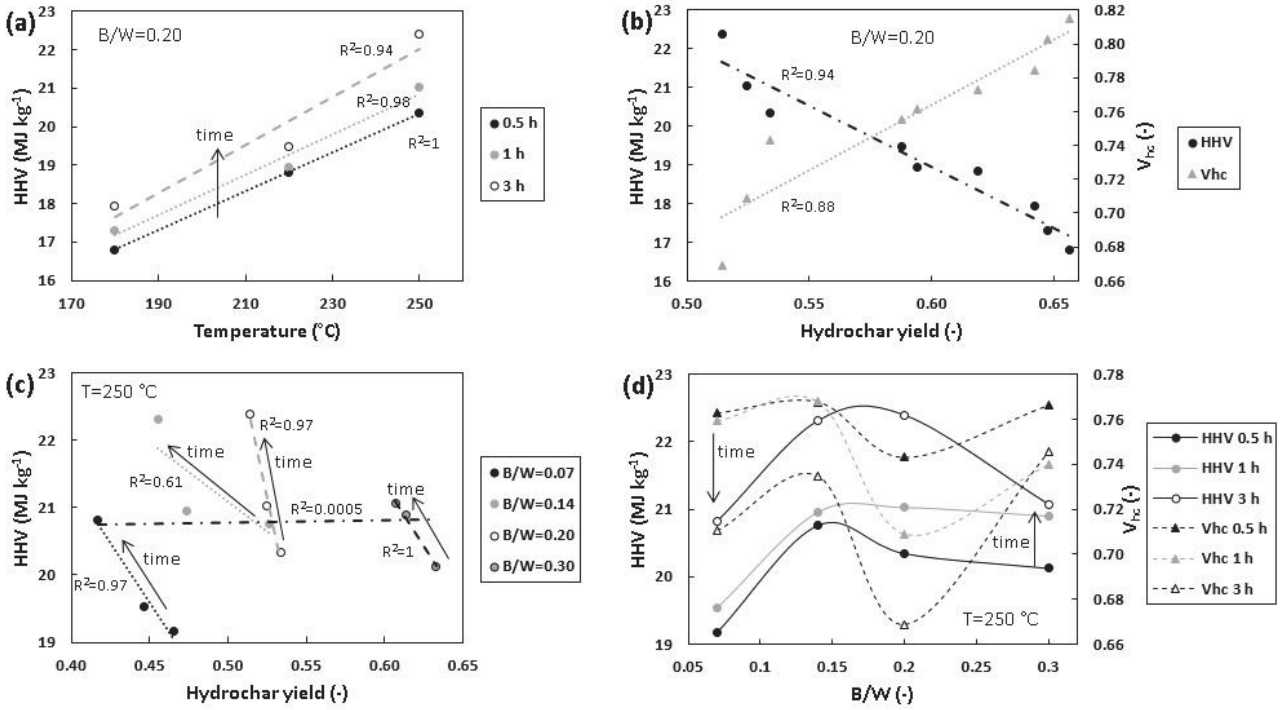

Fig. 3. Dependence of the hydrochar higher heating value and volatility on process variables. (a) HHV vs. temperature at B/W=0.20 and different reaction times, linear trendlines with R^2 are reported; (b) HHV and V_{HC} vs. hydrochar yield at B/W=0.20 and different reaction temperatures and times, linear trendlines with R^2 are reported; (c) HHV vs. hydrochar yield at T=250 °C and different B/W and times, linear trendlines with R^2 are reported; (d) HHV and V_{HC} vs. B/W at T=250 °C and different reaction times, the curves connecting the indicators are intended to help the reader in the comprehension of the figure.

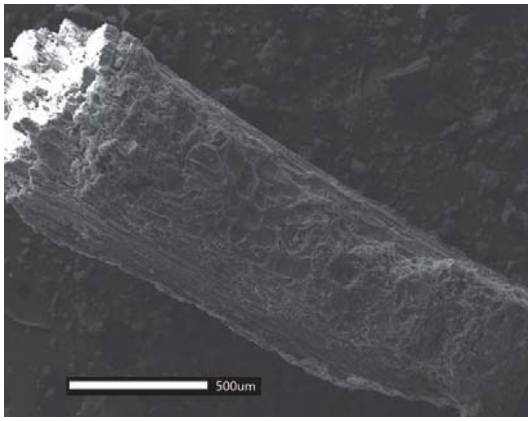

a. 180 °C, 3h, B/W=0.20; scale bar= 500µm

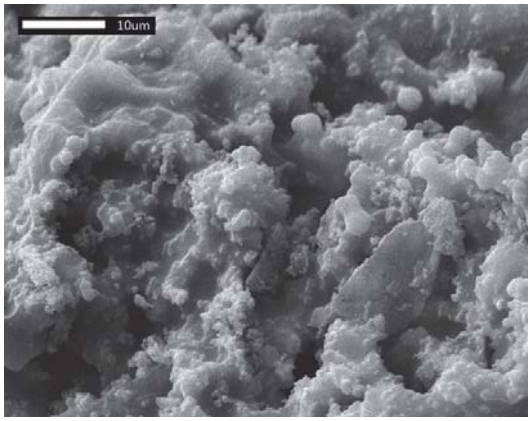

b. 250 °C, 0.5 h, B/W=0.20; scale bar=10µm

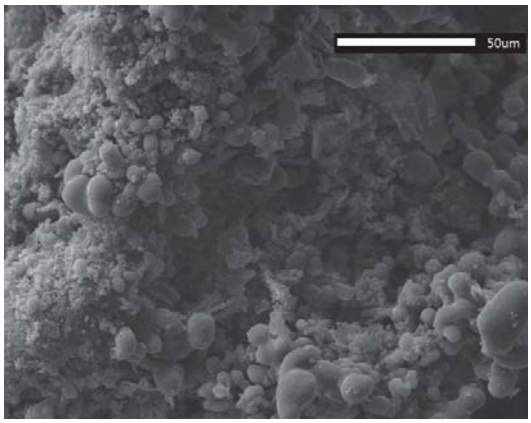

c. 250 °C, 3h, B/W=0.20; scale bar = 50 µm

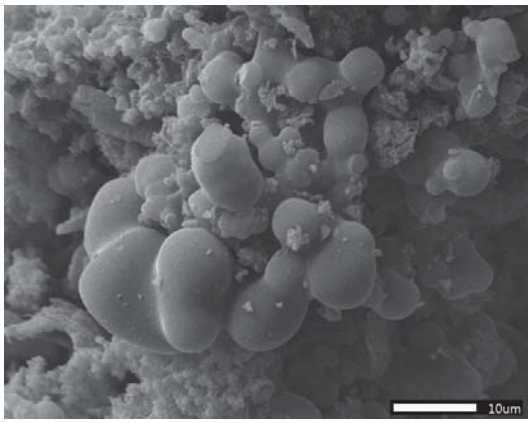

d. 250 °C, 3h, B/W=0.20; scale bar = 10 µm

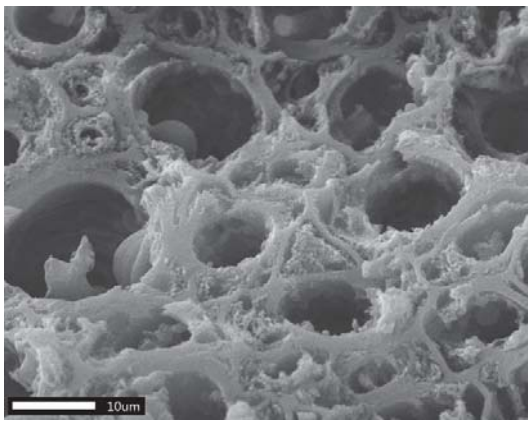

e. 250 °C, 3h, B/W=0.20, extracted with MeOH+Acetone; scale bar = xx µm

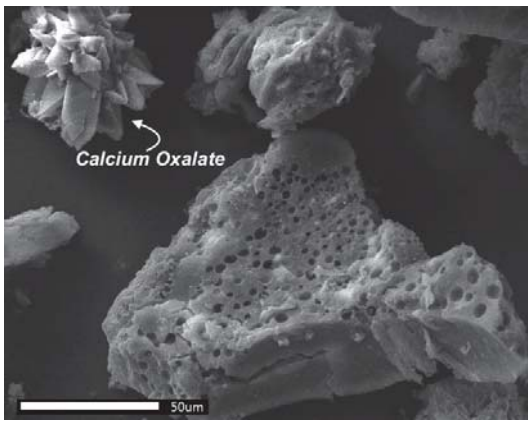

f. 250 °C, 3h, B/W=0.20, extracted; with calcium oxalate detected; scale bar = 50µm

Fig. 4. Scanning electron microscopy images of OC hydrochars (additional images available in SI).

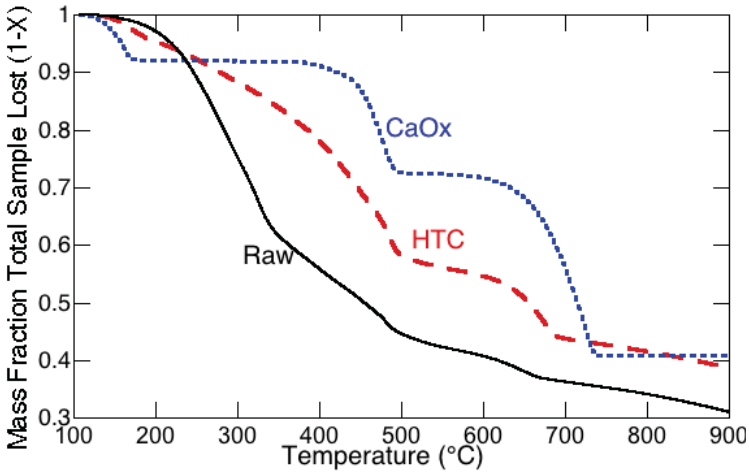

a. Thermogravimetric curves (mass fraction sample lost)

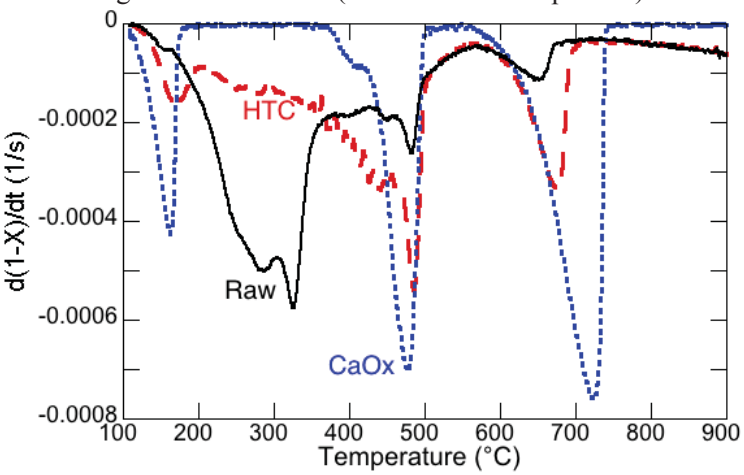

b. Derivative thermogravimetric curves (rate of total mass fraction converted, $X=(m_i-m_t)/m_i$ used to determine relative decomposition of CaOx; see SI for additional analysis)

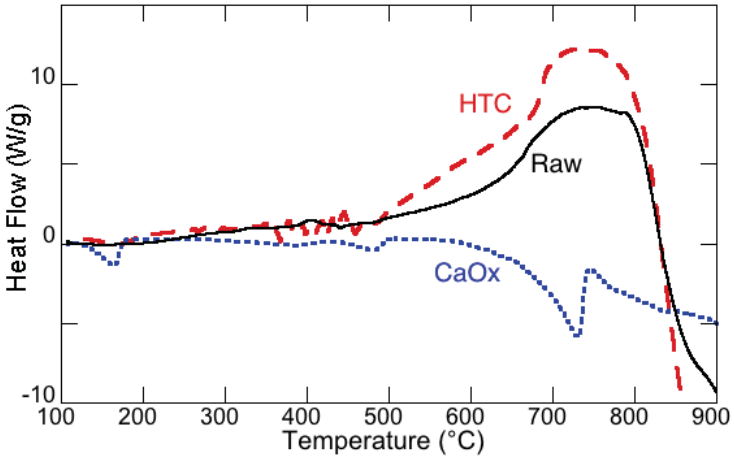

c. Differential scanning calorimetery curves (heat flow normalized to sample mass)

Fig. 5. Thermal analysis of raw OC, HTC (250 °C, 3 h, B/W=0.20) and $CaC_2O_4 \bullet H_2O$ (CaOx) at 5 °C/min in N_2 atmosphere.

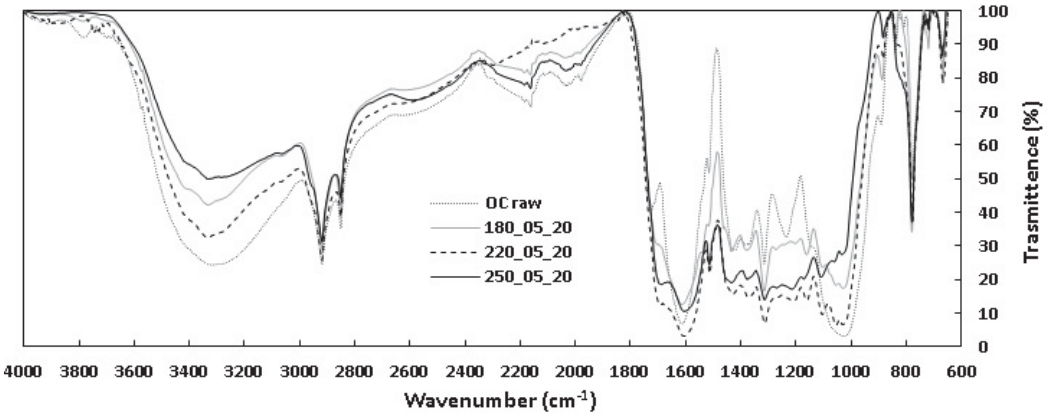

a. Spectra for samples produced at 0.5 h at varying carbonization temperatures

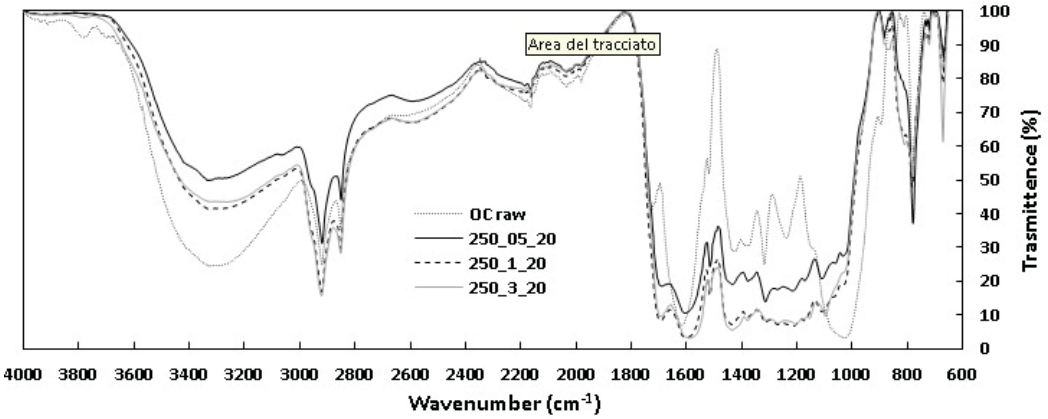

b. Spectra for samples produced at 250°C at varying reaction times

Fig. 6. FTIR spectra of raw biomass and hydrochars at B/W=0.20.

Supplementary information

Click here to download Electronic Annex: Supplementary_info.docx